Optik 127 (2016) 3629–3632

Contents lists available at ScienceDirect

Optik

journal homepage: www.elsevier.de/ijleo

Optical field distribution on a hohlraum wall during indirect laser-driven inertial confinement fusion

Lei Ren*, Kewei You, Zhaoyang Jiao, Jianqiang Zhu

National Laboratory on High Power Laser and Physics, Shanghai Institute of Optics and Fine Mechanics, Chinese Academy of Science, No. 390, Qinghe Road, Jiading District, Shanghai 201800, China

ARTICLE INFO

Article history:
Received 9 September 2015
Accepted 28 December 2015

Keywords:
Optical field distribution
Hohlraum target
Quadruplet beams
ICF

ABSTRACT

A model to calculate the optical field distribution of quadruplet beams on a hohlraum target wall is presented. This model combines geometrical ray tracing, coordinate transformation, and Fresnel diffraction integral to capture the quadruplet beams propagating in four different directions and the typically non-planar geometry of the hohlraum wall. The results demonstrate that the optical field distribution arises mainly from individual beam diffraction, and the interference with other beams in the quadruplet hardly devotes to the distribution. A movie is also produced to interpret the spatio and temporal evolution of the optical field on a cylindrical hohlraum wall.

1. Introduction

In indirect laser-driven inertial confinement fusion (ICF) [1,2], lasers are focused on the inner wall of a hohlraum target to generate X-rays, which more uniformly irradiate a target pellet. Laser beams in typical giant high-power laser drivers, such as those at the National Ignition Facility (NIF) [3] and the Laser Mégajoule (LMJ) Project [4], propagate grouped together, usually in a 2×2 quadruplet, or quad. Different quads are focused into the target hohlraum through different final optics assemblies (FOAs) [5], which are distributed on the target chamber at different polar and azimuthal angles. In this manner, the target hohlraum is more completely and uniformly irradiated. As shown in Fig. 1, one quad is focused at the center of the laser entrance hole (LEH) to irradiate the hohlraum wall; the beam spot on the wall appears as four separated spots instead of the desired single whole beam spot. To develop the best optical design of the target area, and the hohlraum target design, itself, requires analysis of the size, profile, and spacing between the individual spots and the optical field distribution within the beam spots. Such analysis will allow researchers to better understand the beam spots in the hohlraum wall, leading to improved laser driver design and X-ray generation processes.

Two issues make analytically calculating the beam spots difficult. First, the hohlraum target used in indirect driven ICF is typically a cylindrical hohlraum [6], a rugby hohlraum [7], or a spherical hohlraum [8,9]. As shown in Fig. 1, the cross-section of the beam quad and the cylindrical hohlraum is not a plane. Second, a wedged focus lens (WFL) is introduced in the FOA to focus and chromatically separate the beams [5]. The WFL directs the quad beams in separate directions from each other. Further, the four entrance planes of the WFL are not in the same plane. These issues make it difficult to calculate the optical field distribution on the inner wall of the hohlraum using existing beam propagating algorithms.

Jiao [10] reported a method combining a fast Fourier transform (FFT) with chromatography to calculate the spatio-temporal optical field distribution characteristics on a cylindrical hohlraum wall. However, their simulation modeled only one beam and chromatography principles do not suit the optical distribution generated by four beams propagating in four different directions. Studies on the beam conditions of the focus spots in both the NIF and LMJ [11,12] have been published. The plane used to detect the focus spot were all in planes perpendicular to the quad, and not a realistic hohlraum target wall surface, which is usually non-planar and has a certain angle with the quad. In this article, a model combining optical ray tracing and Fresnel diffraction integrals is proposed to calculate the beam spot generated by quad beams on the hohlraum wall. This model is not limited to the cylindrical hohlraum, but can calculate the optical distribution on spherical and other geometrically shaped targets.

2. Model and calculations

In calculating the conventional diffraction pattern of an optical field distribution on a plane [13], the calculating plane and the

* Corresponding author. Tel.: +86 02169918809.
E-mail address: leir89@siom.ac.cn (L. Ren).

http://dx.doi.org/10.1016/j.ijleo.2015.12.121
0030-4026/

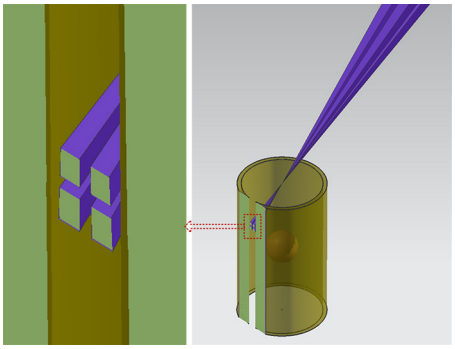

Fig. 1. Schematic of laser quad entrance into the hohlraum target. The beam spots appear as four distinct spots.

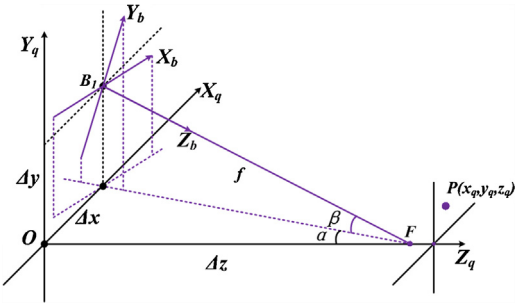

Fig. 3. Transformation relationships between QCS($O-X_qY_qZ_q$) and BCS($B_1-X_bY_bZ_b$). Distances between the quad center, beam center, and LEH center were Δx, Δy, and Δz. The lens rotated α and β degrees along Y_q and X_q axes, respectively. Focus length of the WFL f.

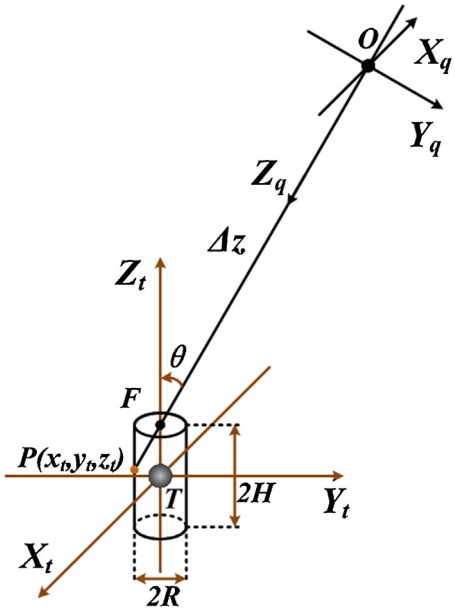

Fig. 2. Transformation relationships between TCCS($T-X_tY_tZ_t$) and QCS($O-X_qY_qZ_q$). Hohlraum diameter 2R and total length 2H. Polar angle θ.

laser emission plane must be parallel to each other. While in a quad, the emergence planes of the four laser beams are not coplanar with each other, or with the calculating plane on the hohlraum wall. Therefore, some modifications to the conventional calculations were required to calculate the optical field distribution with FFT [14]. First, the profile and shape of the beam spots on the hohlraum wall are obtained by a geometrical ray tracing method. The points in the area defined by the beam spots are then transformed into the four laser beam coordinate systems in two-step coordinate transformations. In each individual beam coordinate system, the optical field value of each transformed point is calculated by FFT. Finally, the actual optical field of the original point on the hohlraum wall is calculated as the interference of the four field values. This procedure is applied to each point in the originally defined area to acquire the whole beam spot optical field distribution.

The detailed calculation proceeds as follows: The target chamber coordinate system (TCCS), $T-X_tY_tZ_t$ is taken as the reference coordinate system. The hohlraum is a cylinder with the diameter $2R$ and total length $2H$. Each quad has its own quad coordinate system (QCS), $O-X_qY_qZ_q$. Fig. 2 shows the position and rotating relationship between TCCS and QCS of the quad with the polar angle θ focused at LEH center F of the target hohlraum. Each quad has four different beam coordinate systems (BCSs); Fig. 3 illustrates the beam in the first quadrant, as an example. Its coordinate $B_1-X_bY_bZ_b$ can be transformed to QCS by translation and rotation. The transformation relationships between the three coordinate systems can be expressed as Eqs. (2-1) and (2-2), where Δx and Δy are the x and y translations, respectively, between the quad center and beam center, and Δz is the distance between the quad center and the LEH center. The focus length of the WFL f relates to these translation values as $f=\sqrt{(\Delta x)^2+(\Delta y)^2+(\Delta z)^2}$. A thin lens rotated α and β degrees along Y_q and X_q axes, respectively, simulates the simultaneous focusing and chromatic separation of the beams by the WFL, where $\tan\alpha=\Delta x/\Delta z$ and $\sin\beta=\Delta y/f$. The coordinates of a point in all three systems are (x_t, y_t, z_t), (x_q, y_q, z_q), and (x_b, y_b, z_b), respectively.

$$\begin{bmatrix}\cos\alpha & -\sin\alpha\sin\beta & -\sin\alpha\cos\beta\\ 0 & \cos\beta & -\sin\beta\\ \sin\alpha & \cos\alpha\sin\beta & \cos\alpha\cos\beta\end{bmatrix}\begin{bmatrix}x_b\\ y_b\\ z_b\end{bmatrix}=\begin{bmatrix}x_q-\Delta x\\ y_q-\Delta y\\ z_q\end{bmatrix} \quad (2\text{-}1)$$

$$\begin{bmatrix}-1 & 0 & 0\\ 0 & \cos\theta & -\sin\theta\\ 0 & -\sin\theta & -\cos\theta\end{bmatrix}\begin{bmatrix}x_t\\ y_t\\ z_t-H\end{bmatrix}=\begin{bmatrix}x_q\\ y_q\\ z_q-\Delta z\end{bmatrix} \quad (2\text{-}2)$$

We calculated the beam spot optical field distribution of the FOA [5] in the outer cone of the NIF target chamber as an example. The polar angle was $\theta=50^\circ$; the distances between the quad center, beam center, and LEH center were $\Delta x=278.3$ mm, $\Delta y=316.25$ mm, and $\Delta z=7688.47$ mm; and focus length was $f=7700$ mm. The hohlraum target was cylindrical, with $R=2.5$ mm and $H=5$ mm. The laser had a wavelength $\lambda=351$ nm, beam size 400 mm × 400 mm, and a 10-order super Gaussian beam with waist radius $\omega=200$ mm.

All parameters were first transformed into TCCS, and underwent ray tracing. The resulting beam spot shape and profile are shown in Fig. 4. The calculating area was defined to cover the total beam spots area, indicated by the red dotted rectangle in Fig. 4. Each point in the calculating area was transformed from TCCS coordinates, to QCS, and then into all four BCS, $B_i-X_{bi}Y_{bi}Z_{bi}$, $i=1, 2, 3, 4$. For $P(X_{bi},Y_{bi},Z_{bi})$ in BCS, the optical field distribution in the plane $z=Z_{bi}$ can be easily calculated by FFT. However, the point (X_{bi},Y_{bi}) was not necessarily one of the sample dots in the plane $z=Z_{bi}$, so 2D interpolation was performed to acquire the precise optical field. The final optical intensity distribution on the hohlraum wall, shown in Fig. 5, was calculated by interfering the optical fields from the four BCSs.

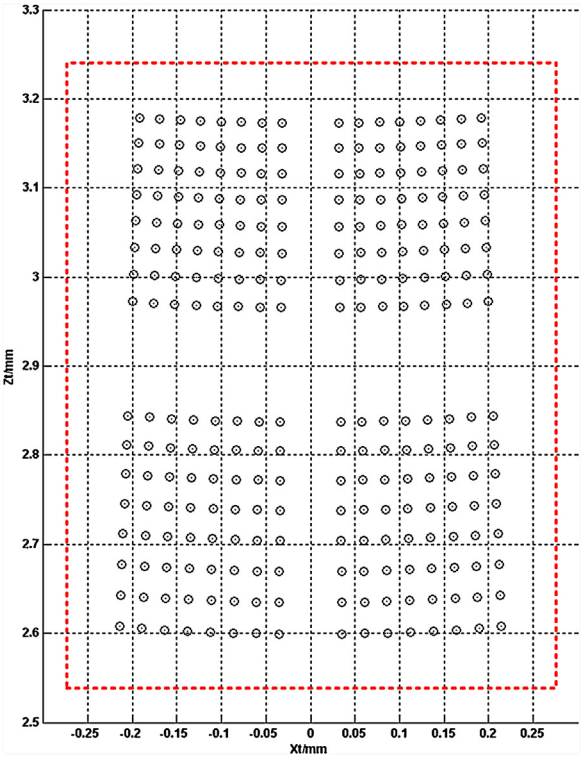

Fig. 4. Profile and shapes of the beam spots obtained by the ray tracing method. The red rectangle is the defined range covering all the beam spots. (For interpretation of the references to color in this figure legend, the reader is referred to the web version of this article.)

The final intensity distribution results from diffraction of individual beams and interference between quad beams. In Fig. 5, diffraction was evident in the significant intensity differences within each beam, while interference can hardly been observed, for the quad lasers were too separated that they had little effects on the optical distribution of each beam.

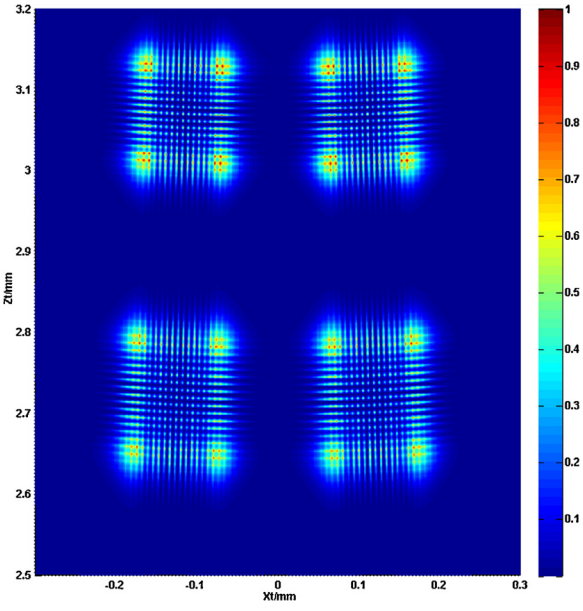

Fig. 5. Intensity distribution on the hohlraum wall, viewed along Y_t axis.

3. Discussion

3.1. Effects of polar angles

The quad beams in all four cones on the target chamber can be calculated by this method. In order to clearly observe the effect of polar angle on intensity distributions on the hohlraum, we varied the polar angles and graphed the results in the same plot, shown in Fig. 6. As the incident angles decreasing from 50.0° to 23.5°, both the optical spots areas and the interval distances among the four beams become larger and larger, so the intensities in the inner cones (23.5° and 30°) are obviously lower than the outer cones (44.5° and 50°). However, there are 32 quads in the outer cones and 16 quads in the inner cones, so the generated X-ray densities will not be uniform between inner and outer cones, which will affect the irradiation to the target pellet in the hohlraum.

3.2. Spatio and temporal evolution of the optical field

When considering the temporal characteristics of the laser pulse, 50-order super-Gaussian pulses with pulse width of 3 ns and a rising edge of approximately 200 ps is taken as an example. According to the hohlraum size and the distance between the center of LEH and beam quad, it takes about 2 ps for the quad beams to evolve its beam spot in the inner wall of the hohlraum, as shown in Fig. 7, which was extracted from a movie on this 2 ps evolution process. Because the evolution time is far less than the rising edge, the intensity of the laser is supposed to be constant during the evolution.

Consider another situation where the evolution time is much longer than the pulse width, for example an ultra-short laser pulse with pulse width of 15 fs. The pulse is too fast to evolve the complete beam spot that there will be only four lines in the hohlraum wall instead of the four spots. Therefore, to obtain higher power in the

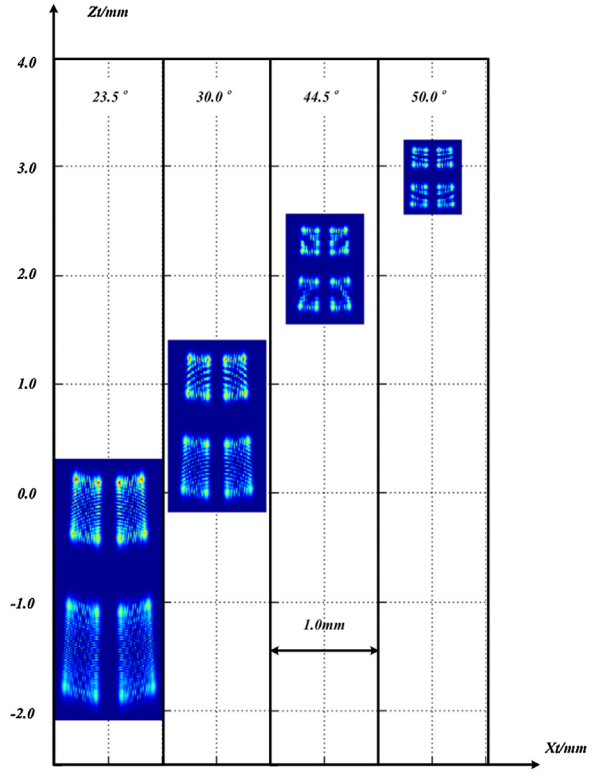

Fig. 6. The intensity distributions on hohlraum wall by quads with different polar angles.

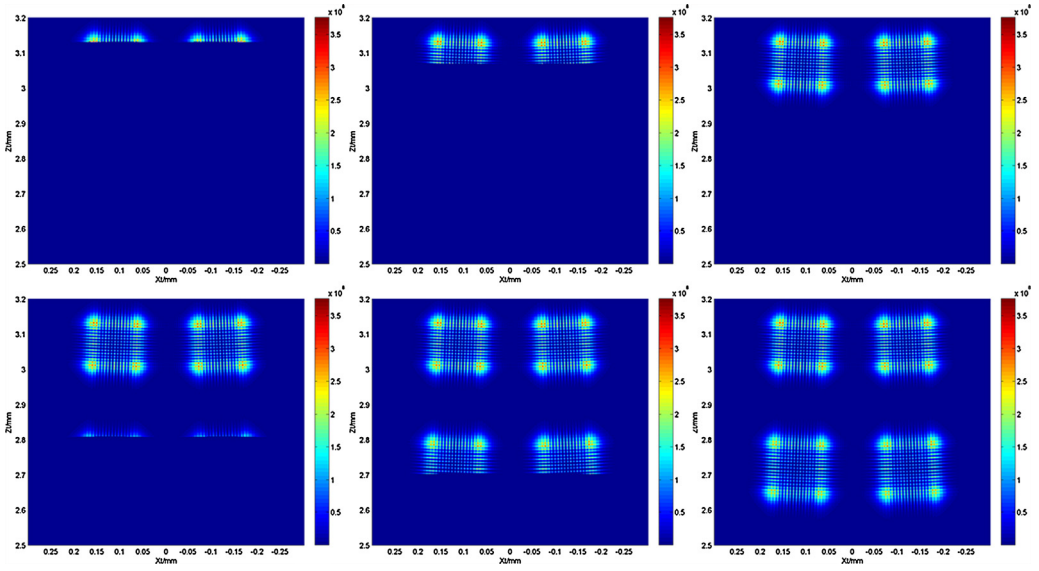

Fig. 7. Spatio and temporal evolution of the optical field on a cylindrical hohlraum wall.

target wall with Peta-Watt laser beam combination, both the target and the manner of laser shooting the target need to be carefully designed.

4. Conclusions

A model was proposed to calculate the intensity distribution of quad beams focused on a hohlraum target wall. Although it was found to arise from both individual beam diffraction and interference between beams in the quad, individual diffraction dominated the distribution. According to the calculation of different NIF quads, inner cones had lower intensity in the hohlraum wall than that of outer cones. However, only 1/3 of the total quads were attributed to inner cones and that maybe not conducive to the uniform irradiation to the target pellet. The spatio and temporal evolution of the optical field in the hohlraum wall was demonstrated by a short movie. Given the evolution time and pulse width, the 2×2 quadruplet beam combination was not suitable for the ultra-short pulse laser to obtain higher power in the hohlraum.

Acknowledgements

The authors would like to acknowledge Dr. C. Wang, Dr. P. Zhu, Dr. Z. J. Cui, and Professor W. B. Pei for their great help and kind discussion.

References

[1] J.D. Lindl, P. Amendt, R.L. Berger, S.G. Glendinning, S.H. Glenzer, S.W. Haan, R.L. Kauffman, O.L. Landen, L.J. Suter, The physics basis for ignition using indirect-drive targets on the National Ignition Facility, Phys. Plasmas 11 (2004) 339–491.
[2] J. Nuckolls, A. Thiessen, L. Wood, G. Zimmerma, Laser compression of matter to super-high densities—thermonuclear (CTR) applications, Nature 239 (1972) 139-&.
[3] C.A. Haynam, P.J. Wegner, J.M. Auerbach, M.W. Bowers, S.N. Dixit, G.V. Erbert, G.M. Heestand, M.A. Henesian, M.R. Hermann, K.S. Jancaitis, K.R. Manes, C.D. Marshall, N.C. Mehta, J. Menapace, E. Moses, J.R. Murray, M.C. Nostrand, C.D. Orth, R. Patterson, R.A. Sacks, M.J. Shaw, M. Spaeth, S.B. Sutton, W.H. Williams, C.C. Widmayer, R.K. White, S.T. Yang, B.M. Van Wonterghem, National ignition facility laser performance status, Appl. Opt. 46 (2007) 3276–3303.
[4] P. Vivini, M. Nicolaizeau, The LMJ: overview of recent advancements and very first experiments, High Power Lasers for Fusion Research III vol. 9345 (2015).
[5] P. Wegner, J. Auerbach, T. Biesiada, S. Dixit, J. Lawson, J. Menapace, T. Parham, D. Swift, P. Whitman, W. Williams, NIF final optics system: frequency conversion and beam conditioning, in: M.A. Lane, C.R. Wuest (Eds.), Optical Engineering at the Lawrence Livermore National Laboratory II: The National Ignition Facility, Proceedings of SPIE, vol. 5341, SPIE, Bellingham, WA, 2004, pp. 180–189.
[6] S.W. Haan, J.D. Lindl, D.A. Callahan, D.S. Clark, J.D. Salmonson, B.A. Hammel, L.J. Atherton, R.C. Cook, M.J. Edwards, S. Glenzer, A.V. Hamza, S.P. Hatchett, M.C. Herrmann, D.E. Hinkel, D.D. Ho, H. Huang, O.S. Jones, J. Kline, G. Kyrala, O.L. Landen, B.J. MacGowan, M.M. Marinak, D.D. Meyerhofer, J.L. Milovich, K.A. Moreno, E.I. Moses, D.H. Munro, A. Nikroo, R.E. Olson, K. Peterson, S.M. Pollaine, J.E. Ralph, H.F. Robey, B.K. Spears, P.T. Springer, L.J. Suter, C.A. Thomas, R.P. Town, R. Vesey, S.V. Weber, H.L. Wilkens, D.C. Wilson, Point design targets, specifications, and requirements for the 2010 ignition campaign on the National Ignition Facility, Phys. Plasmas 18 (2011) 051001.
[7] P. Amendt, D.D. Ho, O.S. Jones, High-density carbon ablator ignition path with low-density gas-filled rugby hohlraum, Phys. Plasmas 22 (2015) 040703.
[8] K. Lan, J. Liu, D. Lai, W. Zheng, X.-T. He, High flux symmetry of the spherical hohlraum with octahedral 6LEHs at the hohlraum-to-capsule radius ratio of 5.14, Phys. Plasmas 21 (2014) 010704.
[9] J.M. Wallace, T.J. Murphy, N.D. Delamater, K.A. Klare, J.A. Oertel, G.R. Magelssen, E.L. Lindman, A.A. Hauer, P. Gobby, J.D. Schnittman, R.S. Craxton, W. Seka, R. Kremens, D. Bradley, S.M. Pollaine, R.E. Turner, O.L. Landen, D. Drake, J.J. MacFarlane, Inertial confinement fusion with tetrahedral hohlraums at OMEGA, Phys. Rev. Lett. 82 (1999) 3807–3810.
[10] Z. Jiao, Y. Zhang, J. Zhang, J. Zhu, Spatio-temporal evolution of the optical field on a hohlraum wall at the rising edge of a flat-topped pulse, High Power Laser Sci. Eng. 1 (2013) 88–93.
[11] J.M. Di-Nicola, N. Fleurot, T. Lonjaret, X. Julien, E. Bordenave, B. Le Garrec, M. Mangeant, G. Behar, T. Chies, C. Féral, H. Graillot, M. Luttmann, F. Jequier, E. Journot, O. Lutz, G. Thiell, The LIL facility quadruplet commissioning, J. Phys. IV (Proceedings) 133 (2006) 595–600.
[12] U.S. Lawrence Livermore Natl Lab, National Ignition Facility User Guide, U.S. Lawrence Livermore Natl Lab, 2012.
[13] J.W. Cooley, J.W. Tukey, An algorithm for machine calculation of complex fourier series, Math. Comput. 19 (1965) 297-&.
[14] D. Mas, J. Garcia, C. Ferreira, L.M. Bernardo, F. Marinho, Fast algorithms for free-space diffraction patterns calculation, Opt. Commun. 164 (1999) 233–245.